ACS APPLIED MATERIALS & INTERFACES

www.acsami.org

Forum Article

Ionic Covalent Organic Framework Membrane as Active Separator for Highly Reversible Zinc−Sulfur Battery

Published as part of ACS Applied Materials & Interfaces special issue "Celebrating the 110th Anniversary of the College of Chemistry, Chemical Engineering, and Materials Science of Soochow University".

Liyao Wang, Yan Xu,* Linyu Xiao, Yang Liu, Lixinyu Wang, Shangwen Zha, Shenxiang Zhang,* and Jian Jin*

Cite This: *ACS Appl. Mater. Interfaces* 2024, 16, 50036−50044

Read Online

ACCESS | Metrics & More | Article Recommendations | Supporting Information

ABSTRACT: Zinc-sulfur (Zn-S) batteries exhibit a high theoretical energy density, nontoxicity, and cost-effectiveness, demonstrating significant potential for integration into large-scale energy storage systems. However, the phenomenon of polysulfide (including dissolved S_8 and S_x^{2-}) shuttling is a major issue that results in rapid capacity decay and a short lifespan, limiting the practical performance of sulfur-based batteries. Herein, we fabricated an ionic covalent organic framework (iCOF) membrane as an active separator for the Zn-S battery. Sulfonic acid groups were introduced to the COF membrane, providing abundant negative charge sites in its pore wall. By combining size sieving and charge interaction between the polysulfide and pore wall, the iCOF membrane inhibited the crossover of polysulfides to the Zn metal anode without affecting the transport of metal ions. The Zn-S battery with the iCOF membrane as the separator shows a high-performance and low attenuation rate of 0.05% per cycle over 300 cycles at 2.5 A g^{-1}. This study emphasizes the significance of separator design in enhancing Zn-S batteries and showcases the potential of functionalized framework materials for the development of high-performance energy storage systems.

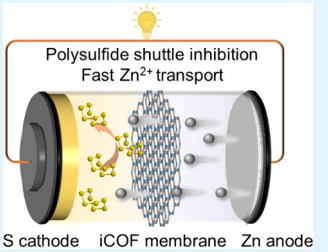

KEYWORDS: *covalent organic framework, ionic membrane, battery separator, zinc−sulfur battery, polysulfide shuttle effect*

1. INTRODUCTION

Large-scale energy storage systems for the electric grid require active materials with high energy density and low costs.[1−3] The sulfur (S) cathode material is a promising option because it is abundant and affordable and has an impressive theoretical capacity of 1675 mA h g^{-1}.[4−7] There has been substantial focus on using sulfur in metal-sulfur batteries, such as lithium-sulfur, sodium-sulfur, and magnesium-sulfur batteries, to access its high energy capacity. Recently, zinc (Zn) has gained attention in battery development due to its 820 mAh g^{-1} theoretical capacity, low redox potential (−0.76 V vs standard hydrogen electrode), low cost, and good compatibility with most organic/aqueous electrolytes.[8−14] When the high-capacity S cathode is combined with the Zn metal anode, along with an equilibrium voltage of 0.95 V, it results in a high energy density of over 500 Wh kg^{-1} (based on Zn and S).[15,16] These characteristics make them strong candidates for developing next-generation energy storage devices.[17]

Although S is a highly promising cathode material for large-scale energy storage, the phenomenon of polysulfide shuttling is a major issue that limits the practical performance of sulfur-based batteries.[18,19] Polysulfides, such as S_8, and S_x^{2-} (x = 8, 6, or 4) could dissolve in liquid electrolytes (Figure S1a and S1b), resulting in sulfide migration from the cathode to the anode. When polysulfides dissolved in the electrolyte come into contact with the surface of the metal anode, they initiate irreversible reactions, forming a sulfur-containing interface. This adversely affects the reversibility of metal stripping and plating.[20] For instance, in the case of Zn-S batteries, the reaction between soluble polysulfides and the Zn anode creates a solid-electrolyte interphase containing S on the surface of Zn (Figure S2), leading to reduced mobility of Zn^{2+} and increased interfacial resistance. On the other hand, the loss of active material not only causes capacity decay but also leads to parasitic reactions, contributing to rapid battery degradation. Preventing polysulfide shuttling is crucial for improving the performance of Zn-S batteries.

Affective strategies include tuning the electrolyte solvation structure to reduce the intrinsic solubility of polysulfides and adsorption within cathode material to impede the diffusion of dissolved polysulfides into electrolytes.[21−23] This can be accomplished through chemical or physical interactions of polysulfide species with a barrier material, such as porous

Received: July 10, 2024
Revised: September 2, 2024
Accepted: September 2, 2024
Published: September 12, 2024

https://doi.org/10.1021/acsami.4c11422
ACS Appl. Mater. Interfaces 2024, 16, 50036−50044

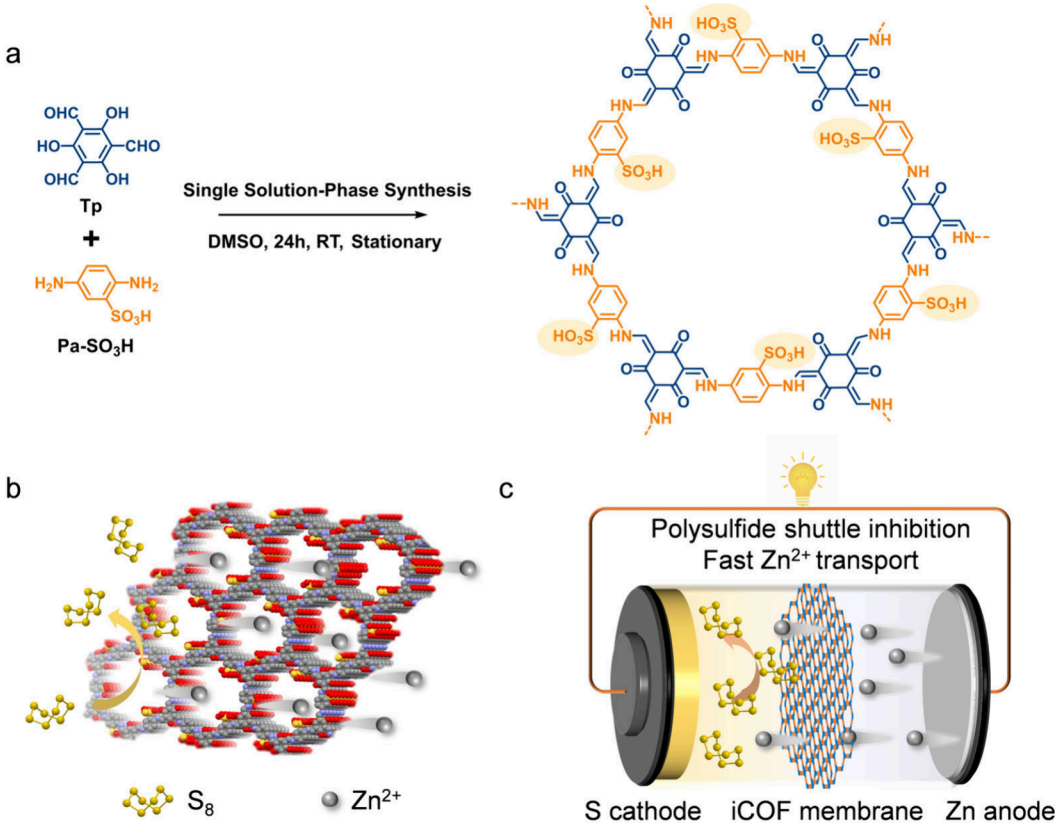

Figure 1. Schematic illustration of the synthesis and usage of iCOF membrane as the separator in Zn-S battery. (a) The synthesis of iCOF. (b) Schematic diagram of iCOF membrane allowing fast Zn^{2+} transport and blocking of polysulfide. (c) Schematic diagram of the Zn-S battery with iCOF separator.

carbon materials,[16,24] framework materials,[25] metal oxides,[26] and sulfur-based polymers.[27,28] Although using a blocking material in metal-S batteries can partly suppress polysulfide shuttling, it is also possible that the slow Zn^{2+} diffusion due to the high charge density of Zn^{2+} results in the accumulation of Zn^{2+} in the lattice. Once the accumulated Zn^{2+} in the host material reaches a critical amount, some irreversible phase transitions occur, leading to capacity loss and slow kinetic processes.[29] An alternative strategy to overcome this challenge is to use a membrane to separate electrolyte phases (such as anolyte and catholyte) and prevent the crossover of polysulfides.[30] A polymer membrane,[31−33] such as sulfonated styrene, sulfonated polyethylene, and Nafion, containing sulfonic acid functional groups, can naturally repel polysulfides and reduce chemical crossover to the metal anode. However, the incorporation of a denser polymer membrane as a separator invariably results in undesirable impedance to metal ion transport. Furthermore, the diminished diffusion of metal ions hampers the reactivation of the S-based cathode material, leading to decreased reaction kinetics and specific capacity. Hence, there is a pressing need for a selective separator capable of impeding the transport of polysulfide without affecting the transport of metal ions.

Covalent organic frameworks (COFs) are attractive, innovative membrane materials with intrinsic nanopores and structural tunability.[34] They are characterized by uniform pore size, high porosity and good stability.[35] The chemical arrangement of molecular building blocks allows for the creation of pore chemistry and structure in COFs, which could be utilized in the realm of energy storage. Additionally, the robust structure of COFs allows them to withstand severe operating conditions, ensuring battery cycle stability.[36,37]

Herein, we fabricated an ionic COF (iCOF) membrane as an active separator for the Zn-S battery. First, ultrathin iCOF nanosheets were synthesized by reacting 2,5-diaminobenzenesulfonic acid (Pa-SO_3H) with 1,3,5-triformylphloroglucinol (Tp) to polymerize in a single solution phase (Figure 1a).[38] Second, iCOF membranes were prepared by vacuum filtering the iCOF nanosheets onto a porous substrate to form a lamellar structure with adjustable thickness. The sulfonic acid groups in the COF membrane provide abundant negative charge sites in its pore wall, which achieve a selective cation permeability and polysulfides blocking (Figure 1b). When working as an active barrier in a Zn-S battery, mass transport between the anolyte and catholyte is regulated by the pore and interlayer channels in the iCOF membrane through the synergistic effects of size sieving and charge interaction. The crossover of polysulfides (including dissolved S_8 and S_x^{2-}) to the metal Zn anode was inhibited by the iCOF membrane, without affecting the transport of metal ions (Figure 1c). By this design, the Zn-S battery, using the iCOF membrane as the separator, demonstrates a high-performance multiplicity and an extremely low attenuation rate of 0.05% per cycle over 300 cycles at a current density of 2.5 A g^{-1}.

2. EXPERIMENTAL SECTION

2.1. Materials and Chemicals. 1,3,5-Triformylphloroglucinol (Tp, ≥97%) was purchased from Bide Co., Ltd. 2,5-Diaminobenzenesulfonic acid (Pa-SO_3H, >98%) was purchased from Aladdin. Dimethyl sulfoxide (DMSO, 99%), sulfolane (≥99.5%) and ethylene glycol (EG, 98%) were purchased from MACKLN Co., Ltd.

https://doi.org/10.1021/acsami.4c11422
ACS Appl. Mater. Interfaces 2024, 16, 50036−50044

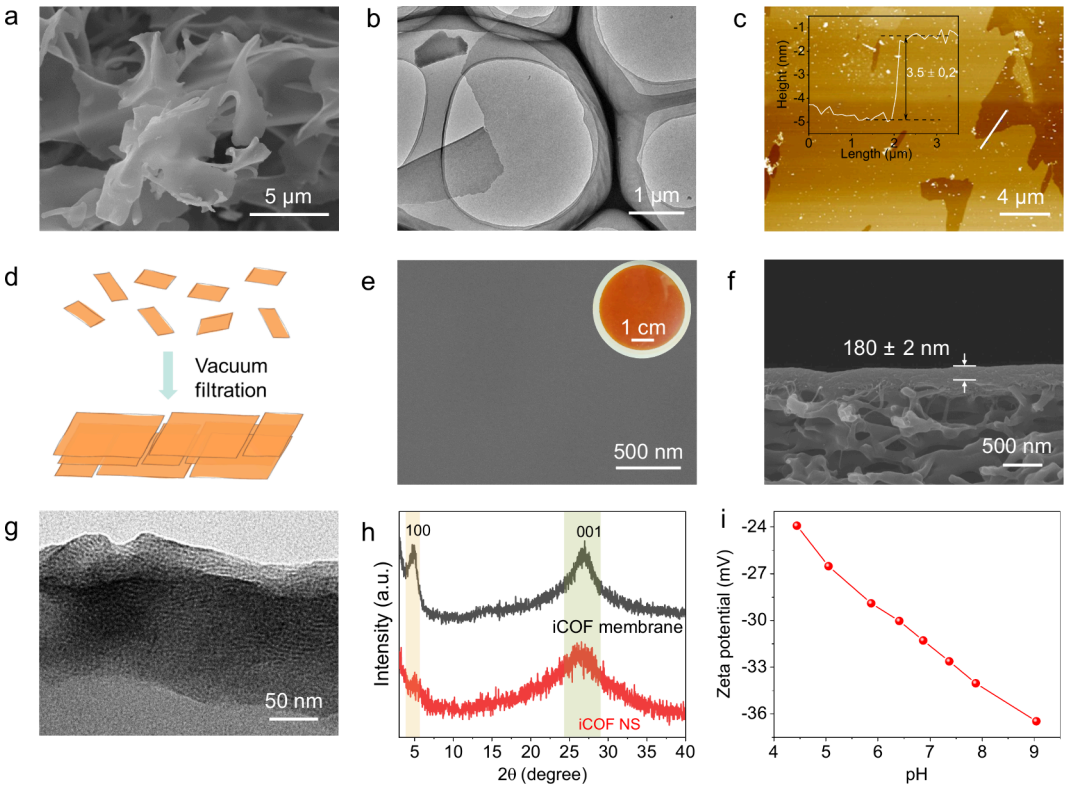

Figure 2. Morphology and structure characterization of iCOF nanosheets and iCOF membrane. (a) SEM, (b) TEM and (c) AFM of iCOF nanosheets. (d) Schematic diagram of the fabrication of iCOF membrane by vacuum filtration method. (e) Surface morphology, (f) cross-sectional SEM and (g) TEM of iCOF membrane. (h) XRD of the iCOF nanosheets and iCOF membrane. (i) The zeta potential of iCOF membrane.

Deionized (DI) water was prepared by a Milli-Q water purifier (18.2 MΩ cm, Millipore). Dialysis tube (MD77, MWCO 30 kDa) was supplied by Suke Co., Ltd. The polyether sulfone (PES) microfiltration substrate with an average pore size of 0.22 μm was purchased from Yibo Co., Ltd.

2.2. Synthesis of iCOF Nanosheets. Pa-SO_3H (42.0 mg, 0.2 mmol) and Tp (56.5 mg, 0.3 mmol) were dissolved in 5.0 mL of DMSO, respectively. The Tp solution was dropped into the Pa-SO_3H solution with mild stirring. The mixed solution was left at room temperature for 24 h. Then, the product was dialyzed with a dialysis tube (molecular weight cutoff of 30 kDa) in water for 3 days to remove unreacted monomers and DMSO solvent. Finally, a iCOF nanosheet dispersion was obtained with a concentration of about 4 mg mL^{-1}.

2.3. Preparation of iCOF Membrane on Single-Wall Carbon Nanotube (SWCNT) Substrate. The SWCNT substrate was prepared according to our previous report.[39,40] Specifically, 2 mL of SWCNT dispersion (concentration: 0.024 mg mL^{-1}) was diluted with DI water (50 mL) and vacuum-filtered onto the PES microfiltration membrane with a pore size of 0.22 μm at 0.1 bar of vacuum pressure to form a SWCNT substrate. A certain amount of iCOF nanosheets dispersion was added to 50 mL of DI water. And then, the iCOF nanosheets dispersion was filtrated on the prepared SWCNT substrate. The thickness of the iCOF membrane was controlled by tuning the amount of the iCOF nanosheets dispersion. The obtained iCOF membrane was heated in an oven at 60 °C for 1 h.

2.4. Preparation of S/Carbon Cathodes. Sulfur was loaded in active carbon (AC3000) by a melt-diffusion method. In brief, 1.0 g of sulfur powder and 1.0 g of AC3000 were thoroughly mixed by grinding and then sealed in a Teflon-lined autoclave. The autoclave was heated at 155 °C for 12 h. The S@AC3000 powder, Ketjenblack, and PTFE were blended with a mass ratio of 6:3:1 and added to an ethanol solvent. Then the slurry was stirred for 30 min and then spread onto carbon paper and dried at 60 °C for 12 h. The areal sulfur loading in the resultant cathode is around 1.0 mg cm^{-2}.

2.5. Instruments and Characterizations. The morphology of the iCOF nanosheets and membrane was captured with a field emission scanning electron microscope (SEM, Hitachi S8230). The surface element distribution was measured by energy-dispersive X-ray spectroscopy (EDX). A transmission electron microscope (TEM, FEI Tecnai F20) was used to characterize the cross-sectional morphology of the iCOF membrane. The thickness of the iCOF nanosheets was measured by an atomic force microscope (AFM, Dimension Icon, Bruker). X-ray diffraction (XRD) measurements were recorded on a Bruker D8 instrument equipped with Cu Kα of wavelength λ = 1.54 Å. The scan speed was set as 2° min^{-1}. The surface area and pore size distributions of iCOF were measured by N_2 adsorption using a Quantachrome Autosorb-iQ instrument. Before the measurement, samples were degassed at 120 °C under vacuum for 12 h. The zeta potential of the iCOF membrane was characterized with an electrokinetic analyzer (Sur-PASS 3, Anton Paar, GmbH). In S_8 and S_4^{2-} permeation tests, the concentration of S_8 and S_4^{2-} was measured by UV−vis spectrophotometry (UV2600i, SHIMADZU). The electrochemical performance of Zn-S batteries was tested by using Land instruments (Wuhan LAND Electronics Co., Ltd.). The cyclic voltammetry (CV) and electrochemical impedance spectroscopy (EIS) tests were performed on an electrochemical working station (CHI660E).

2.6. Zinc Ion Transference Number Measurement. The transference number of Zn^{2+} was evaluated in a symmetric Zn cell using a chronoamperometry (CA) test in 2.0 M $ZnSO_4$ electrolyte. The constant step potential was set as 10 mV, and the Zn^{2+} transference number was calculated from the ratio of steady state current to initial state current according to eq 1:

$$t_{Zn^{2+}} = \frac{I_s}{I_0} \tag{1}$$

where $t_{Zn^{2+}}$ is the Zn^{2+} transference number and I_s and I_0 represent the current at the steady state and initial state, respectively.

https://doi.org/10.1021/acsami.4c11422
ACS Appl. Mater. Interfaces 2024, 16, 50036−50044

2.7. Ionic Conductivity Measurement. The ionic conductivity of the iCOF membrane was measured in a 2.0 M $ZnSO_4$ electrolyte using an EIS (0.01 mHz to 100 kHz) method with a symmetrical cell composed of two Cu foils. The ionic conductivity was calculated according to eq 2:

$$\sigma = \frac{L}{R_b \times A} \quad (2)$$

where σ is the ionic conductivity (S cm^{-1}) and L, R_b and A represent the thickness of the separator (cm), bulk resistance (Ω), and area of the stainless-steel electrode (cm^2), respectively.

2.8. Battery Electrochemical Performance Measurement. CR2032-type coin cells were assembled consisting of a sulfur cathode, an iCOF membrane, and a Zn foil anode. The electrolyte was composed of 344 mg of lithium bis(trifluoromethanesulphonyl)imide (LiTFSI), 436 mg of zinc trifluoromethanesulphonate ($Zn(OTf)_2$), and 1.0 mg of I_2, all dissolved in a 1.2 mL mixture of H_2O/EG/sulfolane (volume ratio 2:1:1). For comparison, the coin cell with the glass fiber as the separator was also assembled. The charge/discharge voltage range was set in the range of 0.25−1.55 V. The rate performance was tested by varying the current density from 1.0 to 5.0 A g^{-1}.

3. RESULTS AND DISCUSSION

3.1. Fabrication and Characterization of iCOF Membrane. The COF membrane was synthesized via a Schiff-base condensation reaction of 1,3,5-triformylphloroglucinol (Tp) and 2,5-diaminobenzenesulfonic acid (Pa-SO_3H) in a dimethyl sulfoxide solution following a previous report.[41] Figure 2a displays the SEM image of the iCOF nanosheets, which exhibit a two-dimensional (2D) sheet structure with a width exceeding ten microns. TEM analysis revealed that the iCOF nanosheets were thin, micrometer-sized, large monolithic sheets (Figure 2b). The iCOF nanosheets were transferred onto a mica sheet, and AFM measurements indicated a thickness of 3.5 ± 0.2 nm (Figure 2c). The chemical structure of the iCOF nanosheets was confirmed by using Fourier transform infrared spectroscopy (FT-IR) and solid-state ^{13}C nuclear magnetic resonance (^{13}C NMR) spectra. A shift of carbonyl signals from 1635 cm^{-1} in Tp to 1572 cm^{-1} in iCOF nanosheets was observed, along with the disappearance of the characteristic N-H signal (3300−3400 cm^{-1}) in the Pa-SO_3H monomer and the appearance of stretching signals at 1221 cm^{-1} (C-N), suggesting the successful fabrication of TpPa-SO_3H iCOF nanosheets. (Figure S3). Additionally, the presence of a (C═O) peak at approximately 180 ppm in the solid ^{13}C NMR spectrum suggests the formation of COFs as the keto form (Figure S4).

Figure 2d illustrates a schematic diagram of the iCOF membrane preparation process. To prevent the iCOF nanosheet from penetrating the PES membrane, a porous SWCNT film was fabricated as a substrate (SEM images; see Figure S5). The iCOF membrane was fabricated on a porous SWCNT substrate through vacuum filtration of a 50 mL dispersion containing specific concentrations of iCOF nanosheets (0.004, 0.008, and 0.016 mg mL^{-1}, respectively). The obtained iCOF membranes were denoted as iCOF-X nm, where X presents the thickness of the membrane. The SEM analysis revealed that the iCOF membrane has a continuous, smooth surface without any cracks (Figures 2e, S6a and S6b). The thicknesses of the iCOF membranes were 90 ± 2 nm, 180 ± 2 nm, and 380 ± 5 nm, as measured from cross-sectional SEM images, respectively (Figures 2f, S6c and S6d). The cross-sectional morphology of the iCOF-180 nm membrane was observed by using TEM, which revealed that the membrane consisted of stacked nanosheets (Figure 2g). This stacking of nanosheets may further reduce the pore size of the membrane with the increasing of membrane thickness.

The structure of the obtained iCOF nanosheets and membrane was investigated by XRD. In Figure 2h, the diffraction patterns of both iCOF nanosheets and the iCOF membrane exhibited two distinct diffraction peaks at 4.6° and 27°. These peaks correspond to the (100) and (001) crystal planes, respectively.[42,43] As for the iCOF membrane, the intensity of the peaks at 4.6° and 27° is higher than that of the iCOF nanosheets, indicating that the iCOF membrane has a more orderly stack. A N_2 adsorption experiment at 77 K was conducted to analyze the pores in iCOF (Figure S7). The adsorption isotherm displays a pronounced increase in the relative pressure range below 0.02, which can be identified as a type I sorption isotherm, indicative of a microporous structure. The Brunauer−Emmett−Teller (BET) surface area was estimated to be 21.7 m^2 g^{-1}, and the pore size distribution analysis was calculated based on the nonlocal density functional theory (NLDFT) cylindrical pore model (Figure S7, inset). The results indicate that the pore size of the iCOF nanosheets is predominantly concentrated at 1.4 nm. Thermogravimetric analysis (TGA) was used to examine the thermal stability of the iCOF nanosheets. The analysis indicated that no significant weight loss occurred prior to 260 °C (Figure S8), showing the structural integrity of iCOF nanosheets.

During the operation of the Zn-S batteries, the wettability of the electrolyte to the separators has an important influence on the electrochemical performance. As shown in Figure S9, the electrolyte exhibits a strong affinity for the iCOF membrane, with the dynamic contact angle rapidly declining from 41.0° to 11.7° within 19.5 s. This phenomenon is primarily attributed to the strong affinity between the negatively charged iCOF membrane and the polar molecules present in the electrolyte. The surface charging characteristics were further studied by using the surface zeta potential test. Figure 2i shows that the iCOF membrane has a strong negative value of −31.7 mV. The increased negative charge of the iCOF membrane is due to the electron-donating nature of the sulfonic acid group, which helps block negatively charged polysulfides through electrostatic repulsion. Moreover, the membrane was also highly stable in the electrolyte (Figure S10).

3.2. Selective Transport Performance of iCOF Membrane. To comprehensively assess the impact of the iCOF membrane on Zn^{2+} transport behavior, the ionic conductivity and Zn^{2+} transfer number were measured. Based on Figure 3a, a symmetrical Cu-Cu cell was constructed using a 180 nm-thick iCOF membrane. This cell demonstrated an ionic conductivity of 18.22 mS cm^{-1}, slightly surpassing that of the GF (18.11 mS cm^{-1}). Furthermore, the iCOF membrane demonstrated a Zn^{2+} transference number of 0.15, only 0.02 lower than the GF separator (Figure 3b). These results suggest comparable Zn^{2+} conducting capabilities between the iCOF and the GF separator, attributed to the negatively charged sulfonic acid groups on the pore wall facilitating the Zn^{2+} transport.[44−46]

Permeation tests were conducted in an H-type cell to explore the impediment ability of the iCOF membrane toward polysulfides. The feed side was filled with polysulfide solution, and the permeate side was filled with fresh solvent (inset in Figure 3c). The concentration of polysulfide in the permeate side was measured by UV−vis spectrophotometry. The

https://doi.org/10.1021/acsami.4c11422
ACS Appl. Mater. Interfaces 2024, 16, 50036−50044

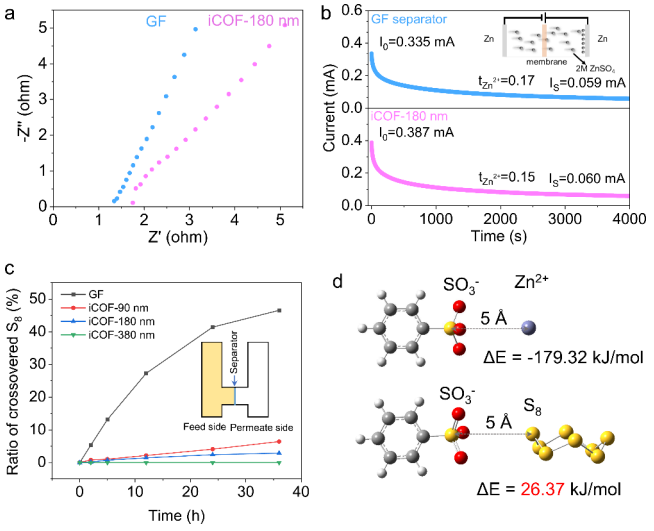

Figure 3. Selective transport performance of iCOF membrane. (a) Impedance plots and (b) chronoamperometric curves of symmetrical Zn−Zn cell with a 180 nm-thick iCOF membrane as separator. (c) S8 diffusion curve with GF, iCOF-90 nm, iCOF-180 nm, and iCOF-380 nm working as a separator. Inset is schematic diagram of H-type cell for the permeation test. (d) Mechanism understandings on the fast transport of Zn^{2+} while blocking polysulfide and the Gibbs free energies between the sulfonic acid group and Zn^{2+}, S8.

impediment ability of the GF separator toward polysulfides was also investigated for comparison. Approximately 48.5% of S_8 passed through the GF separator within 36 h (Figures 3c and S11), indicating that the GF separator cannot prevent the transfer of dissolved S_8. In contrast, only 6.4% and 2.8% of S_8 transferred through the iCOF-90 nm and iCOF-180 nm after 36 h, respectively. Additionally, no S_8 transferred through to the right side when iCOF-380 nm was a separator. In Li-S, Na-S, or Mg-S battery systems, the crossover of S_x^{2-} (x = 8, 6, or 4) is quite common. Here we also investigated the impediment ability of the iCOF membrane toward Na_2S_4. As shown in Figures S12−S14, approximately 5.0% of the polysulfides permeated the bare GF membrane within 12 h. When the iCOF-90 nm worked as a separator, 0.4% of S_4^{2-} permeated to the right side after 12 h. With the increase of membrane thickness to 180 and 380 nm, no S_4^{2-} permeated to the right side, even after 240 h. These results demonstrate that when the iCOF membrane with a thickness higher than 180 nm, iCOF membrane can effectively inhibit the crossover of polysulfides. To better understand the reason for the impediment ability toward polysulfides, the Gibbs free energies between the sulfonic acid group and Zn^{2+}, S_8, and S_4^{2-} were calculated based on density functional theory (DFT, for detailed calculation method see eq S1 and Table S1). At a fixed distance of 5 Å, the Gibbs free energy between the sulfonic acid group and Zn^{2+} is −179.32 kJ mol^{-1} (Figure 3d), indicating that the transfer of Zn^{2+} is thermodynamically feasible. However, at the same fixed distance of 5 Å, the Gibbs free energies between the sulfonic acid group and S_8 or S_4^{2-} are 26.37 and 34.39 kJ mol^{-1}, respectively (Figures 3d and S14b). This indicates that the sulfonic acid group has an exclusionary effect toward polysulfides. These results demonstrate that by combining size sieving and charge interaction between the polysulfide and pore wall, the iCOF membrane inhibited the crossover of polysulfides to the Zn metal anode without affecting the transport of metal ions.

3.3. Electrochemical Performance of the Zn-S Battery Using iCOF Separator. The electrochemical performance of the Zn-S battery at different scan rates (0.1−0.6 mV s^{-1}) was used to investigate the dynamic behavior and Zn^{2+} diffusion characteristics of the Zn-S battery. The discharge and charge behavior in the range 0.25−1.55 V was studied by CV. It can be seen from the CV curve in Figure 4a that the anode and

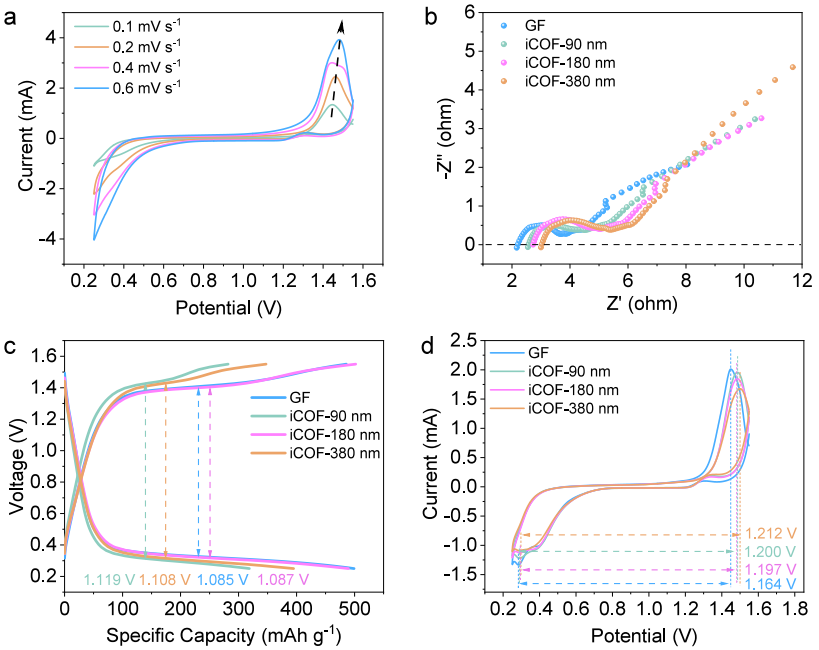

Figure 4. Ion conductivity behaviors iCOF membrane in Zn-S battery. (a) CV profiles of Zn-S batteries at different scan rate with iCOF-180 nm as a separator. (b) EIS curves of Zn-S batteries with iCOF membrane or GF as a separator. (c) Charge−discharge voltage profiles at 2.5 A g^{-1}. (d) CV comparison at the scan rate of 0.1 mV s^{-1}.

https://doi.org/10.1021/acsami.4c11422
ACS Appl. Mater. Interfaces 2024, 16, 50036−50044

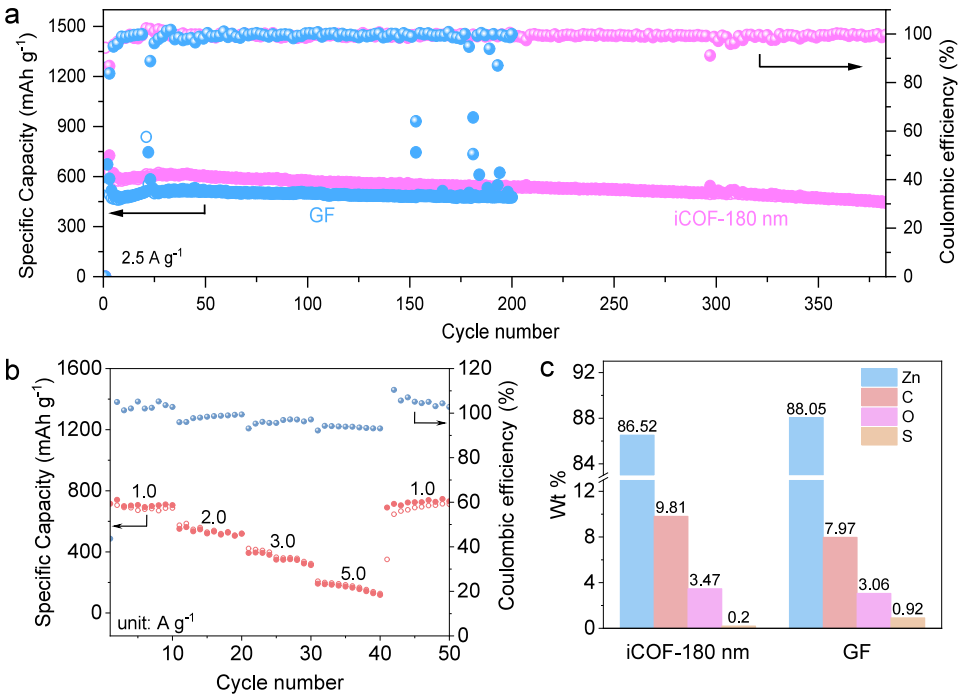

Figure 5. Battery performance. (a) Cycle performance of Zn-S battery-equipped iCOF-180 nm membrane and GF as separator at a current density of 2.5A g^{-1}. (b) Rate performances of the iCOF membrane batteries. (c) Elemental composition analysis of the zinc anodes in the Zn-S battery, utilizing iCOF-180 nm and GF as separators, was conducted after 100 cycles.

cathode scans showed obvious oxidation and reduction peaks, respectively. The variation trend of the peak current is the same as that of the scan rate, and their highly correlated relationship is verified from the linear fitting results (Figure S15), showing a good ionic diffusion rate. EIS was recorded further to investigate the interfacial resistance (Figure 4b). When iCOF-180 nm is used as a separator, the charge transfer resistance is 2.7 Ω, which is 0.5 Ω higher than that of GF (2.2 Ω), within an acceptable range.

The discharge and charge electrochemical performance of Zn-S batteries with different thicknesses of iCOF separators were further evaluated. As shown in Figure 4c, the Zn-S battery with the iCOF-180 nm membrane as separator has the largest capacity and the smallest potential difference compared with other thicknesses of the iCOF membrane, indicating that it is electrochemically active. In addition, from the CV curve at a scan rate of 0.1 mV s^{-1} (Figure 4d), compared with the cells using iCOF-90 nm and iCOF-380 nm as separators, the cell using iCOF-180 nm as separator has a polarization voltage of 1.197 V closer to that of GF, which further proves the superior kinetics of the redox conversion reaction.

Based on the synergistic effect of the barrier effect on polysulfides and the effect on battery polarization, iCOF-180 nm was selected as the separator to explore the long cycle and rate performance of the Zn-S battery. Figure 5a presents the cycling performance of Zn-S batteries using iCOF-180 nm and GF as separators at a current density of 2.5 A g^{-1}. Benefiting from the ability to block polysulfides, the initial average discharge capacity of the Zn-S battery using iCOF-180 nm as separator was 613.7 mAh g^{-1} and the capacity retention rate was still 92.4% after 150 cycles. The maximum cycle life is 384 cycles with an average Coulombic efficiency (CE) of 99.8%. In contrast, the initial discharge capacity of the GF-based battery was 507.7 mAh g^{-1} and charge−discharge imbalance occurred after 150 cycles; the CE also fluctuated greatly, reflecting the formation of a passivation layer due to the polysulfide shuttle effect. Comparison of the specific capacity and cycling performance of this Zn-S battery with those of previously reported Zn-S batteries is presented in Table S2. The incorporation of the iCOF membrane as a barrier yields competitive performance compared with the state-of-the-art Zn-S battery.

The rate capabilities of the iCOF membrane were investigated at various current densities from 1.0 to 5.0 A g^{-1} (Figure 5b). The discharge-specific capacity of the battery was 699.3, 533.0, 349.0, and 175.0 mAh g^{-1} at 1.0, 2.0, 3.0, and 5.0 A g^{-1}, respectively. In addition, the discharge-specific capacity could be restored to 694.6 mAh g^{-1} (99.3% of the retention rate) when it was returned to 1.0 A g^{-1} after running at different current densities, which meant that it had excellent stability at different current densities. The corresponding constant current discharge and charge curves of the Zn-S battery at different current densities are shown in Figure S16. The results show that the iCOF battery has good polarization suppression ability. These results further confirmed the role of the iCOF membrane as a barrier layer for polysulfides and an accelerator for Zn^{2+}, thereby improving the performance of Zn-S batteries. In addition, the Zn anode of the 100 cycles battery was characterized to investigate the surface element distribution (Figure 5c and S17). The sulfur content on the zinc anode side of the battery without iCOF membrane was 0.92 wt %, which was 4.6 times higher than that with iCOF-180 nm membrane (0.2 wt %). It is further indicated that the inhibition of polysulfides by the iCOF-180 nm membrane increases the cycling stability of the Zn-S battery.

4. CONCLUSIONS

In conclusion, we fabricated thin iCOF membranes and deployed them as active separators in Zn-S batteries. This approach capitalizes on the combined effect of negative charge

https://doi.org/10.1021/acsami.4c11422
ACS Appl. Mater. Interfaces 2024, 16, 50036−50044

repulsion on the membrane surface and the stacking of iCOF nanosheets, leading to a reduction in membrane pore size and effectively impeding the polysulfide shuttle effect. The presence of abundant sulfonic acid groups on the COF pore wall serves as a zinc-philic site, thereby facilitating the migration of Zn^{2+} ions. Zn-S batteries employing this functionalized iCOF membrane have demonstrated exceptional rate performance and cycle stability. This study enhances the performance of Zn-S batteries by concomitantly mitigating the polysulfide shuttle while preserving Zn^{2+} transport. It underscores the promise of membrane materials in advancing next-generation energy storage systems.

■ ASSOCIATED CONTENT

Supporting Information

The Supporting Information is available free of charge at https://pubs.acs.org/doi/10.1021/acsami.4c11422.

UV−vis and Raman spectra of S_8 in the electrolyte; FT-IR and NMR spectra of iCOF nanosheets; SEM images of iCOF membrane; BET surface area plot of iCOF; contact angles and TGA curve of iCOF; UV−vis spectra of polysulfides solutions through separators; photographs demonstrating the permeation of polysulfide through the bare GF separator and the iCOF membrane; EDS mapping of Zn anode after running 100 cycles. (PDF)

■ AUTHOR INFORMATION

Corresponding Authors

Yan Xu − *College of Energy, Soochow Institute for Energy and Materials Innovations, Soochow University, Suzhou, Jiangsu 215123, China*; Email: yanxu2022@suda.edu.cn

Shenxiang Zhang − *College of Chemistry, Chemical Engineering and Materials Science and Jiangsu Key Laboratory of Advanced Functional Polymer Materials and Jiangsu Key Laboratory of Advanced Negative Carbon Technologies, Soochow University, Suzhou, Jiangsu 215123, China*; orcid.org/0000-0003-2857-333X; Email: sxzhang@suda.edu.cn

Jian Jin − *College of Chemistry, Chemical Engineering and Materials Science and Jiangsu Key Laboratory of Advanced Functional Polymer Materials and Jiangsu Key Laboratory of Advanced Negative Carbon Technologies, Soochow University, Suzhou, Jiangsu 215123, China*; orcid.org/0000-0003-0429-300X; Email: jjin@suda.edu.cn

Authors

Liyao Wang − *College of Chemistry, Chemical Engineering and Materials Science, Soochow University, Suzhou, Jiangsu 215123, China*

Linyu Xiao − *College of Chemistry, Chemical Engineering and Materials Science, Soochow University, Suzhou, Jiangsu 215123, China*

Yang Liu − *College of Chemistry, Chemical Engineering and Materials Science, Soochow University, Suzhou, Jiangsu 215123, China*; orcid.org/0000-0002-1789-6937

Lixinyu Wang − *College of Chemistry, Chemical Engineering and Materials Science, Soochow University, Suzhou, Jiangsu 215123, China*

Shangwen Zha − *College of Chemistry, Chemical Engineering and Materials Science, Soochow University, Suzhou, Jiangsu 215123, China; Department of Research and Development, Shanghai ECO Polymer Sci. & Tech. CO., Ltd, Shanghai 201306, China*

Complete contact information is available at: https://pubs.acs.org/10.1021/acsami.4c11422

Author Contributions

S. Zhang, Y. Xu and J. Jin designed the project; L. Wang, Y. Liu, L. X. Wang and L. Xiao synthesized and characterized the membranes and evaluated the battery performance. S. Zha provided suggestions and technical support. L. Wang, S. Zhang and J. Jin wrote and edited the manuscript; J. Jin supervised the project.

Notes

The authors declare no competing financial interest.

■ ACKNOWLEDGMENTS

This work was supported by the National Key Research and Development Program of China (2022YFB3805903), the National Natural Science Foundation of China (22208229, 21988102 and 22309127), the Key Research and Development Plan of Jiangsu Province (BE2022056), the Natural Science Foundation of Jiangsu Province (BK20220501 and BK20230499), General Programs of Jiangsu Province Universities (23KJB150030) and Gusu Innovation and Entrepreneurship Leading Talent Plan (ZXL2023198).

■ REFERENCES

(1) Jia, X.; Liu, C.; Neale, Z. G.; Yang, J.; Cao, G. Active Materials for Aqueous Zinc Ion Batteries: Synthesis, Crystal Structure, Morphology, and Electrochemistry. *Chem. Rev.* **2020**, *120* (15), 7795−7866.

(2) Fang, G.; Zhou, J.; Pan, A.; Liang, S. Recent Advances in Aqueous Zinc-Ion Batteries. *ACS Energy Lett.* **2018**, *3* (10), 2480−2501.

(3) Zhu, Z.; Jiang, T.; Ali, M.; Meng, Y.; Jin, Y.; Cui, Y.; Chen, W. Rechargeable Batteries for Grid Scale Energy Storage. *Chem. Rev.* **2022**, *122* (22), 16610−16751.

(4) Cheng, Q.; Xu, W.; Qin, S.; Das, S.; Jin, T.; Li, A.; Li, A. C.; Qie, B.; Yao, P.; Zhai, H.; Shi, C.; Yong, X.; Yang, Y. Full Dissolution of the Whole Lithium Sulfide Family (Li_2S_8 to Li_2S) in a Safe Eutectic Solvent for Rechargeable Lithium−Sulfur Batteries. *Angew. Chem., Int. Ed.* **2019**, *58* (17), 5557−5561.

(5) Cai, P.; Sun, W.; Chen, J.; Chen, K.; Lu, Z.; Wen, Z. High-Energy Density Aqueous Alkali/Acid Hybrid Zn-S Battery. *Adv. Energy Mater.* **2023**, *13* (28), 2301279.

(6) Liu, J.; Ye, C.; Wu, H.; Jaroniec, M.; Qiao, S.-Z. 2D Mesoporous Zincophilic Sieve for High-Rate Sulfur-Based Aqueous Zinc Batteries. *J. Am. Chem. Soc.* **2023**, *145* (9), 5384−5392.

(7) Cui, M.; Fei, J.; Mo, F.; Lei, H.; Huang, Y. Ultra-High-Capacity and Dendrite-Free Zinc−Sulfur Conversion Batteries Based on a Low-Cost Deep Eutectic Solvent. *ACS Appl. Mater. Interfaces* **2021**, *13* (46), 54981−54989.

(8) Wu, Y.; Zhu, Z.; Shen, D.; Chen, L.; Song, T.; Kang, T.; Tong, Z.; Tang, Y.; Wang, H.; Lee, C. S. Electrolyte Engineering Enables Stable Zn-Ion Deposition for Long-Cycling Life Aqueous Zn-ion Batteries. *Energy Storage Mater.* **2022**, *45*, 1084−1091.

(9) Liu, D.; He, B.; Zhong, Y.; Chen, J.; Yuan, L.; Li, Z.; Huang, Y. A Durable ZnS Cathode for Aqueous Zn-S Batteries. *Nano Energy* **2022**, *101*, 107474.

(10) Mehta, S.; Kaur, S.; Singh, M.; Kumar, M.; Kumar, K.; Meena, S. K.; Nagaiah, T. C. Unleashing Ultrahigh Capacity and Lasting Stability: Aqueous Zinc-Sulfur Batteries. *Adv. Energy Mater.* **2024**, *14*, 2401515.

(11) Liu, S.; Ji, H.; Wang, M.; Sun, H.; Liu, J.; Yan, C.; Qian, T. Atomic Metal Vacancy Modulation of Single-Atom Dispersed Co/N/

C for Highly Efficient and Stable Air Cathode. *ACS Appl. Mater. Interfaces* **2020**, *12* (13), 15298−15304.
(12) Wang, M.; Liu, S.; Xu, N.; Qian, T.; Yan, C. Active Fe-N Sites in Carbon Nanosheets as Oxygen Reduction Electrocatalyst for Flexible All-Solid-State Zinc−Air Batteries. *Adv. Sustainable Syst.* **2017**, *1* (10), 1700085.
(13) Ji, H.; Wang, M.; Liu, S.; Sun, H.; Liu, J.; Hou, Z.; Qian, T.; Yan, C. Identifying the Lewis Base Chemistry in Preventing the Deposition of Metal Oxides on Ketone-Enriched Carbon Cathodes for Highly Durable Metal−Air Batteries. *ACS Appl. Mater. Interfaces* **2020**, *12* (3), 3603−3609.
(14) Meng, Y.; Wang, M.; Xu, J.; Xu, K.; Zhang, K.; Xie, Z.; Zhu, Z.; Wang, W.; Gao, P.; Li, X.; Chen, W. Balancing Interfacial Reactions through Regulating p-Band Centers by an Indium Tin Oxide Protective Layer for Stable Zn Metal Anodes. *Angew. Chem., Int. Ed.* **2023**, *62* (40), No. e202308454.
(15) Wu, W.; Wang, S.; Lin, L.; Shi, H.-Y.; Sun, X. A Dual-Mediator for a Sulfur Cathode Approaching Theoretical Capacity with Low Overpotential in Aqueous Zn-S Batteries. *Energy Environ.* **2023**, *16* (10), 4326−4333.
(16) Amiri, A.; Sellers, R.; Naraghi, M.; Polycarpou, A. A. Multifunctional Quasi-Solid-State Zinc−Sulfur Battery. *ACS Nano* **2023**, *17* (2), 1217−1228.
(17) Yang, M.; Yan, Z.; Xiao, J.; Xin, W.; Zhang, L.; Peng, H.; Geng, Y.; Li, J.; Wang, Y.; Liu, L.; Zhu, Z. Boosting Cathode Activity and Anode Stability of Zn-S Batteries in Aqueous Media Through Cosolvent-Catalyst Synergy. *Angew. Chem., Int. Ed.* **2022**, *61* (42), No. e202212666.
(18) Guo, Y.; Chua, R.; Chen, Y.; Cai, Y.; Tang, E. J. J.; Lim, J. J. N.; Tran, T. H.; Verma, V.; Wong, M. W.; Srinivasan, M. Hybrid Electrolyte Design for High-Performance Zinc−Sulfur Battery. *Small* **2023**, *19* (29), 2207133.
(19) Chen, Q.; Hao, J.; Zhang, S.; Tian, Z.; Davey, K.; Qiao, S.-Z. High-Reversibility Sulfur Anode for Advanced Aqueous Battery. *Adv. Mater.* **2024**, *36* (1), 2309038.
(20) Yoshida, L.; Matsui, Y.; Deguchi, M.; Hakari, T.; Watanabe, M.; Ishikawa, M. Improvement of Lithium−Sulfur Battery Performance by Porous Carbon Selection and LiFSI/DME Electrolyte Optimization. *ACS Appl. Mater. Interfaces* **2023**, *15* (31), 37467−37476.
(21) He, Q.; Liao, X.; Xia, L.; Li, Z.; Wang, H.; Zhao, Y.; Truhlar, D. G. Accurate Binding Energies for Lithium Polysulfides and Assessment of Density Functionals for Lithium−Sulfur Battery Research. *J. Phys. Chem. C* **2019**, *123* (34), 20737−20747.
(22) Wang, M.; Meng, Y.; Sajid, M.; Xie, Z.; Tong, P.; Ma, Z.; Zhang, K.; Shen, D.; Luo, R.; Song, L.; Wu, L.; Zheng, X.; Li, X.; Chen, W. Bidentate Coordination Structure Facilitates High-Voltage and High-Utilization Aqueous Zn-I2 Batteries. *Angew. Chem., Int. Ed.* **2024**, No. e202404784.
(23) Chen, X.; Meng, Y.; Xiao, D.; Qin, L. Empowering the Potassium−Sulfur Battery with Commendable Reaction Kinetics and Capacity Output by Localized High-Concentration Electrolytes. *ACS Appl. Mater. Interfaces* **2024**, *16* (19), 24464−24472.
(24) Li, W.; Wang, K.; Jiang, K. A Low Cost Aqueous Zn-S Battery Realizing Ultrahigh Energy Density. *Adv. Sci.* **2020**, *7* (23), 2000761.
(25) Razaq, R.; Din, M. M. U.; Småbråten, D. R.; Eyupoglu, V.; Janakiram, S.; Sunde, T. O.; Allahgoli, N.; Rettenwander, D.; Deng, L. Synergistic Effect of Bimetallic MOF Modified Separator for Long Cycle Life Lithium-Sulfur Batteries. *Adv. Energy Mater.* **2024**, *14* (3), 2302897.
(26) Zhao, C.; Xu, G.-L.; Yu, Z.; Zhang, L.; Hwang, I.; Mo, Y.-X.; Ren, Y.; Cheng, L.; Sun, C.-J.; Ren, Y.; Zuo, X.; Li, J.-T.; Sun, S.-G.; Amine, K.; Zhao, T. A High-Energy and Long-Cycling Lithium−Sulfur Pouch Cell via a Macroporous Catalytic Cathode with Double-End Binding Sites. *Nat. Nanotechnol.* **2021**, *16* (2), 166−173.
(27) Gross, M. M.; Manthiram, A. Rechargeable Zinc-Aqueous Polysulfide Battery with a Mediator-Ion Solid Electrolyte. *ACS Appl. Mater. Interfaces* **2018**, *10* (13), 10612−10617.
(28) Zhao, Y.; Wang, D.; Li, X.; Yang, Q.; Guo, Y.; Mo, F.; Li, Q.; Peng, C.; Li, H.; Zhi, C. Initiating a Reversible Aqueous Zn/Sulfur Battery through a "Liquid Film. *Adv. Mater.* **2020**, *32* (32), 2003070.
(29) Tang, B.; Shan, L.; Liang, S.; Zhou, J. Issues and Opportunities Facing Aqueous Zinc-Ion Batteries. *Energy Environ.* **2019**, *12* (11), 3288−3304.
(30) Ji, Y.; Liu-Théato, X.; Xiu, Y.; Indris, S.; Njel, C.; Maibach, J.; Ehrenberg, H.; Fichtner, M.; Zhao-Karger, Z. Polyoxometalate Modified Separator for Performance Enhancement of Magnesium−Sulfur Batteries. *Adv. Funct. Mater.* **2021**, *31* (26), 2100868.
(31) Allcorn, E.; Nagasubramanian, G.; Pratt, H. D.; Spoerke, E.; Ingersoll, D. Elimination of Active Species Crossover in A Room Temperature, Neutral pH, Aqueous Flow Battery Using a Ceramic NaSICON Membrane. *J. Power Sources* **2018**, *378*, 353−361.
(32) Liu, J.; Zhou, W.; Zhao, R.; Yang, Z.; Li, W.; Chao, D.; Qiao, S.-Z.; Zhao, D. Sulfur-Based Aqueous Batteries: Electrochemistry and Strategies. *J. Am. Chem. Soc.* **2021**, *143* (38), 15475−15489.
(33) Li, Z.; Lu, Y.-C. Polysulfide-based Redox Flow Batteries with Long Life and Low Levelized Cost Enabled by Charge-Reinforced Ion-Selective Membranes. *Nat. Energy* **2021**, *6* (5), 517−528.
(34) Liu, X.; Wang, J.; Shang, Y.; Yavuz, C. T.; Khashab, N. M. Ionic Covalent Organic Framework-Based Membranes for Selective and Highly Permeable Molecular Sieving. *J. Am. Chem. Soc.* **2024**, *146* (4), 2313−2318.
(35) Wu, M.; Jiang, X.; Meng, Y.; Niu, Y.; Yuan, Z.; Du, S.; Li, X.; Ruan, X.; Xiao, W.; Yan, X.; He, G. A Covalent Organic Framework Membrane with Homo Hierarchical Pores for Confined Reactive Crystallization. *ACS Appl. Mater. Interfaces* **2022**, *14* (3), 4739−4749.
(36) Yin, C.; Li, Z.; Zhao, D.; Yang, J.; Zhang, Y.; Du, Y.; Wang, Y. Azo-Branched Covalent Organic Framework Thin Films as Active Separators for Superior Sodium−Sulfur Batteries. *ACS Nano* **2022**, *16* (9), 14178−14187.
(37) An, Q.; Wang, L.; Zhao, G.; Duan, L.; Sun, Y.; Liu, Q.; Mei, Z.; Yang, Y.; Zhang, C.; Guo, H. Constructing Cooperative Interface via Bi-Functional COF for Facilitating the Sulfur Conversion and Li^+ Dynamics. *Adv. Mater.* **2024**, *36* (4), 2305818.
(38) Huang, T.; Jiang, H.; Douglin, J. C.; Chen, Y.; Yin, S.; Zhang, J.; Deng, X.; Wu, H.; Yin, Y.; Dekel, D. R.; Guiver, M. D.; Jiang, Z. Single Solution-Phase Synthesis of Charged Covalent Organic Framework Nanosheets with High Volume Yield. *Angew. Chem. Inter. Ed.* **2023**, *62* (4), No. e202209306.
(39) Zhang, S.; Wei, X.; Cao, X.; Peng, M.; Wang, M.; Jiang, L.; Jin, J. Solar-Driven Membrane Separation for Direct Lithium Extraction from Artificial Salt-Lake Brine. *Nat. Commun.* **2024**, *15* (1), 238.
(40) Gao, S. J.; Zhu, Y. Z.; Zhang, F.; Jin, J. Superwetting Polymer-Decorated SWCNT Composite Ultrathin Films for Ultrafast Separation of Oil-in-Water Nanoemulsions. *J. Mater. Chem. A* **2015**, *3* (6), 2895−2902.
(41) Pan, W.-X.; Chen, L.; Li, W.-Y.; Ma, Q.; Xiang, H.; Ma, N.; Wang, X.; Jiang, Y.; Xia, F.; Zhu, M. Scalable Fabrication of Ionic-Conductive Covalent Organic Framework Fibers for Capturing of Sustainable Osmotic Energy. *Adv. Mater.* **2024**, *36* (27), 2401772.
(42) Khan, N. A.; Luo, M.; Zha, X.; Azad, C. S.; Lu, J.; Chen, J.; Fan, C.; Rahman, A. U.; Olson, M. A.; Jiang, Z.; Wang, D. Water/Vapor Assisted Fabrication of Large-Area Superprotonic Conductive Covalent Organic Framework Membranes. *Small* **2023**, *19* (42), 2303131.
(43) Wang, X.; Shi, B.; Yang, H.; Guan, J.; Liang, X.; Fan, C.; You, X.; Wang, Y.; Zhang, Z.; Wu, H.; Cheng, T.; Zhang, R.; Jiang, Z. Assembling Covalent Organic Framework Membranes with Superior Ion exchange Capacity. *Nat. Commun.* **2022**, *13* (1), 1020.
(44) Wang, Y.; Li, Q.; Hong, H.; Yang, S.; Zhang, R.; Wang, X.; Jin, X.; Xiong, B.; Bai, S.; Zhi, C. Lean-water hydrogel electrolyte for zinc ion batteries. *Nat. Commun.* **2023**, *14* (1), 3890.
(45) Hong, L.; Wu, X.; Wang, L.-Y.; Zhong, M.; Zhang, P.; Jiang, L.; Huang, W.; Wang, Y.; Wang, K.-X.; Chen, J.-S. Highly Reversible Zinc Anode Enabled by a Cation-Exchange Coating with Zn-Ion Selective Channels. *ACS Nano* **2022**, *16* (4), 6906−6915.

https://doi.org/10.1021/acsami.4c11422
ACS Appl. Mater. Interfaces 2024, 16, 50036−50044

(46) Zhang, L.; Huang, J.; Guo, H.; Ge, L.; Tian, Z.; Zhang, M.; Wang, J.; He, G.; Liu, T.; Hofkens, J.; Brett, D. J. L.; Lai, F. Tuning Ion Transport at the Anode-Electrolyte Interface via a Sulfonate-Rich Ion-Exchange Layer for Durable Zinc-Iodine Batteries. *Adv. Energy Mater.* **2023**, *13* (13), 2203790.

https://doi.org/10.1021/acsami.4c11422
ACS Appl. Mater. Interfaces 2024, 16, 50036−50044